

# Ultrafast Reversal of a Fano Resonance in a Plasmon-Exciton System

Raman A. Shah and Norbert F. Scherer

*Department of Chemistry and The James Franck Institute,  
The University of Chicago, 929 East 57th Street,  
Chicago, Illinois 60637, United States*

Matthew Pelton and Stephen K. Gray\*

*Center for Nanoscale Materials, Argonne National Laboratory,  
9700 South Cass Avenue, Argonne, Illinois 60439, United States*

(Dated: June 17, 2021)

## Abstract

When a two-level quantum dot and a plasmonic metal nanoantenna are resonantly coupled by the electromagnetic near field, the system can exhibit a Fano resonance, resulting in a transparency dip in the optical spectrum of the coupled system. We calculate the nonlinear response of such a system, for illumination both by continuous-wave and ultrafast pulsed lasers, using both a cavity quantum electrodynamics and a semiclassical coupled-oscillator model. For the experimentally relevant case of meV thermal broadening of the quantum-dot transition, we predict that femtosecond pulsed illumination can lead to a reversal of the Fano resonance, with the induced transparency changing into a superscattering spike in the spectrum. This ultrafast reversal is due to a transient change in the phase relationship between the dipoles of the plasmon and the quantum dot. It thus represents a new approach to dynamically control the collective optical properties and coherence of coupled nanoparticle systems.

PACS numbers: 42.50.Pq, 42.50.Ar, 71.35.Cc, 73.20.Mf, 81.07.Ta

A hybrid system of a semiconductor quantum dot (QD) in the near field of a plasmonic metal nanostructure can exhibit qualitatively different optical properties than its individual components [1–3]. For sufficiently strong resonant coupling between the QD exciton and the plasmon, the optical spectrum can exhibit Fano interference [4, 5]: the QD creates a dramatic “dipole-induced transparency,” [6] suppressing absorption and scattering in spite of its relatively meager oscillator strength. A classical model can describe this effect in the linear response limit. Calculating the nonlinear response of the hybrid system requires that the QD, at least, be modeled quantum mechanically. Semiclassical (SC) models that treat the QD as a two-level system have predicted novel nonlinear-optical effects, including a “nonlinear Fano effect” and optical bistability [4, 7–10]. Treating both plasmon and QD quantum mechanically further refines the picture [11–15], predicting in particular a suppression of induced transparency, and of bistability, due to additional dephasing not accounted for in the SC model [13, 16].

These phenomena have all been predicted in the regime of very narrow QD linewidths, on the order of  $10 \mu\text{eV}$ , corresponding to liquid-helium temperatures. Although this can be realistic when QDs are coupled to practically lossless components such as photonic-crystal cavities, absorptive heating may render such temperatures infeasible for QDs coupled to plasmonic nanostructures. We therefore consider here the more experimentally achievable parameter regime of meV QD linewidths.

In this regime, we predict a new nonlinear phenomenon for femtosecond pulsed excitation; namely, for particular fluences the Fano resonance reverses, resulting in a coherently enhanced cross section rather than an induced transparency. This is a dynamical analog of the transition from electromagnetically induced transparency to superscattering [17], arising from a transient change in the phase relationship between the QD and the plasmon. It is thus fundamentally different from the nonlinear Fano effect, a steady-state change in the Fano lineshape arising from the dependence of the QD-plasmon coupling strength on the incident field intensity [4, 12].

Our treatment starts with a quantum-mechanical model of the hybrid system. We follow a previously developed cavity quantum electrodynamics (CQED) formalism [4, 11, 13], extending the previous work to the regime of broader QD linewidths and to consideration of the transient optical response. The underlying basis states are  $|qs\rangle$ , where  $q \in \{0, 1\}$  indexes the QD energy levels and  $s \in \{0, 1, 2, \dots\}$  indexes plasmon energy levels. Lowering

and raising operator pairs for the QD and plasmon are  $(\hat{\sigma}, \hat{\sigma}^+)$  and  $(\hat{b}, \hat{b}^+)$ , respectively. The dipole operators are then  $\hat{\mu}_q = d_q(\hat{\sigma} + \hat{\sigma}^+)$  and  $\hat{\mu}_s = d_s(\hat{b} + \hat{b}^+)$ , where  $d_q$  and  $d_s$  are the transition dipole moments of the QD and plasmon, respectively, and the total dipole operator is  $\hat{\mu} = \hat{\mu}_s + \hat{\mu}_q$ . The evolution of the density operator  $\hat{\rho}(t)$  is governed by

$$\frac{d\hat{\rho}}{dt} = -\frac{i}{\hbar}[\hat{H}, \hat{\rho}] + L(\hat{\rho}) \quad , \quad (1)$$

where  $\hat{H}$  is the system Hamiltonian, and  $L(\hat{\rho})$  is a Lindblad superoperator accounting for dissipation. Specifically,  $\hat{H} = \hat{H}_q + \hat{H}_s + \hat{H}_i + \hat{H}_d$ , where  $\hat{H}_q = \hbar\omega_q\hat{\sigma}^+\hat{\sigma}$  is the QD Hamiltonian,  $\hat{H}_s = \hbar\omega_s\hat{b}^+\hat{b}$  is the plasmon Hamiltonian,  $\hat{H}_i = -\hbar g(\hat{\sigma}^+b + \hat{\sigma}b^+)$  describes plasmon-QD coupling, and  $\hat{H}_d = -E(t)\hat{\mu}$  describes driving by an incident electric field  $E(t)$  [18]. The Lindblad superoperator is [11]

$$L_q(\hat{\rho}) = -\frac{\gamma_1}{2}(\hat{\sigma}^\dagger\hat{\sigma}\hat{\rho} + \hat{\rho}\hat{\sigma}^\dagger\hat{\sigma} - 2\hat{\sigma}\hat{\rho}\hat{\sigma}^\dagger) - \gamma_2(\hat{\sigma}^\dagger\hat{\sigma}\hat{\rho} + \hat{\rho}\hat{\sigma}^\dagger\hat{\sigma} - 2\hat{\sigma}^\dagger\hat{\sigma}\hat{\rho}\hat{\sigma}^\dagger\hat{\sigma}) . \quad (2)$$

The first term describes spontaneous emission with rate  $\gamma_1 = T_1^{-1}$ , and the second term describes dephasing with rate  $\gamma_2 = T_2^{-1}$ . In order to solve Eq. (1), we define a maximum number of plasmons,  $N_s$ , above which the density matrix elements are negligible. Solution then involves integrating  $O(N_s^2)$  coupled ordinary differential equations, or, at steady state,  $O(N_s^2)$  coupled algebraic equations [18]. Once a solution is obtained, the total dipole is calculated according to  $\mu(t) = \text{Tr}(\hat{\rho}(t)\hat{\mu})$ .

A computationally simpler approach is a SC or Maxwell-Bloch model, in which the plasmon dipole,  $\mu_s(t)$ , is treated classically and the QD is treated with Bloch equations [19] or their generalization [20] for its reduced density matrix,  $\rho^{QD}(t)$ :

$$\begin{aligned} \ddot{\mu}_s + \gamma_s\dot{\mu}_s + \omega_s^2\mu_s &= A_s[E + J\mu_q] , \\ \dot{\rho}_1 = \omega_q\rho_2 - \gamma_2\rho_1, \quad \dot{\rho}_2 &= -\omega_q\rho_1 - \frac{2d_q}{\hbar}[E + J\mu_s]\rho_3 - \gamma_2\rho_2 , \\ \dot{\rho}_3 &= \frac{2d_q}{\hbar}[E + J\mu_s]\rho_2 - \gamma_1^{\text{SC}}(\rho_3 + 1) , \end{aligned} \quad (3)$$

where  $E = E(t)$ ,  $\rho_1 = 2\text{Re}\rho_{01}^{QD}(t)$ ,  $\rho_2 = -2\text{Im}\rho_{01}^{QD}(t)$ ,  $\rho_3 = \rho_{11}^{QD}(t) - \rho_{00}^{QD}(t)$ , and  $\mu_q = d_q\rho_1$ . One can relate  $A_s$  to the CQED parameters by solving for the steady state of  $\mu_s$  with  $J = 0$  [18], giving  $A_s = 4\omega_s d_s^2/\hbar$ . Comparing classical and quantum dipole interaction energies gives  $J = \hbar g/(d_q d_s)$  [18]. Eqs. 3 can be numerically integrated with or without the rotating wave approximation [18]; the results are essentially identical for the present problem. The SC model involves the solution of a fixed, small number of ordinary differential equations

regardless of intensity, unlike the CQED model, which becomes computationally costly for large  $N_s$ .

A flaw in the SC model is that an excited QD in the dark cannot couple to the plasmon, but does so in CQED via the Purcell effect [11, 18, 21]. With  $\omega_q = \omega_s$  and  $\gamma_s \gg \gamma_1, \gamma_2$ , and  $g$ , the QD's effective decay constant due to the Purcell effect is [18]  $\gamma_1^{\text{eff}} \approx 4g^2/\gamma_s$ . We therefore term the SC model with  $\gamma_1^{\text{SC}} = \gamma_1$  as the “naïve” SC model, and with  $\gamma_1^{\text{SC}} = \gamma_1^{\text{eff}}$  as the “corrected” SC model.

Having obtained  $\mu(t)$  using either the CQED or SC model, the absorption cross section is found according to [18, 22]:

$$\sigma_{\text{abs}}(\omega) = \frac{k}{\epsilon_0} \text{Im}[\alpha(\omega)], \quad (4)$$

where  $k = \sqrt{\epsilon_{\text{med}}}\omega/c$ , with  $\epsilon_{\text{med}}$  being the relative dielectric constant of the surrounding medium, and

$$\alpha(\omega) = \frac{\int e^{-i\omega t} \mu(t) dt}{\epsilon_{\text{med}} \int e^{-i\omega t} E(t) dt}, \quad (5)$$

where integration is over an optical cycle after steady state is reached or over all time for pulsed excitation. While we discuss absorption cross sections here, scattering spectra exhibit nearly identical trends.

The model parameters are obtained by fitting to spectra for a realistic system calculated with the discrete dipole approximation (DDA) [18, 23]. As illustrated in Fig. 1, two Au prolate spheroids with semi-major and semi-minor axes of 15 nm and 10 nm, respectively, are arranged coaxially with a gap of 6 nm. A 4 nm diameter CdSe QD is placed in the center of the gap. The system is embedded in a medium with dielectric constant  $\epsilon_{\text{med}} = 2.25$ , typical of a polymer or glass. The QD dielectric constant is taken to be a Lorentzian function with center frequency chosen to match the plasmon frequency of the metal nanostructure, and with linewidth corresponding to temperatures of 50 – 100 K [5, 18, 24]. The fitting gives  $\hbar\omega_s = 2.042$  eV,  $d_s = 2990$  D,  $\hbar\gamma_s = 150$  meV;  $\hbar\omega_q = 2.042$  eV,  $d_q = 13.9$  D,  $\hbar\gamma_2 = 1.27$  meV; and  $\hbar g = 10.8$  meV [18]. As seen in Fig. 1, the CQED and SC results are in excellent agreement with each other and in good agreement with the DDA spectrum. The QD spontaneous emission rate is calculated according to  $\gamma_1 = \omega_q^3 \sqrt{\epsilon_{\text{med}}} d_q^2 / (3\pi\epsilon_0 \hbar c^3)$  [25], giving  $\hbar\gamma_1 = 268$  neV or  $T_1 = \gamma_1^{-1} = 2.46$  ns; this, in turn, gives  $\hbar\gamma_1^{\text{eff}} = 3.02$  meV, corresponding to  $T_1^{\text{eff}} = 218$  fs.

We begin by considering steady-state spectra. Fig. 2 shows that the Fano resonance dip

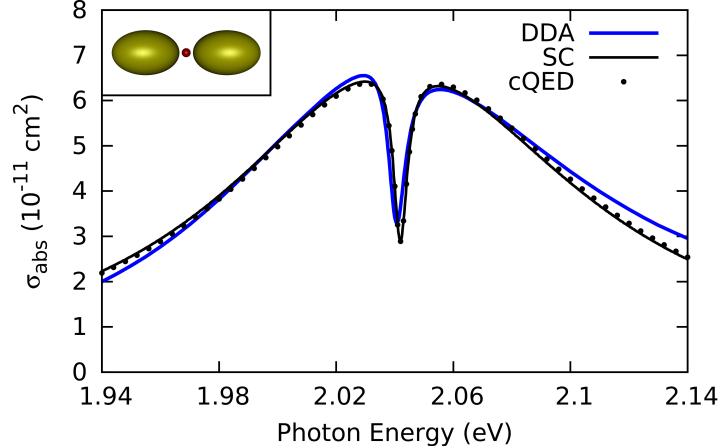


FIG. 1. Linear absorption spectrum of an Au–CdSe–Au hybrid nanoparticle system (illustrated in the inset), calculated using the discrete dipole approximation (DDA), cavity-quantum-electrodynamics model (CQED), and semiclassical model (SC).

disappears as the incident intensity is increased, due to saturation of the QD transition. The corrected SC and CQED models are in excellent quantitative agreement for high and low applied fields. The naïve SC model is gravely in error, but can be brought into agreement with the corrected SC model by multiplying the incident intensity by the Purcell factor [11, 15]. This validates the use of the SC model, which is particularly important for simulations at the high intensities for which CQED calculations are computationally prohibitive. The results for the current system contrast with predictions for systems with narrow QD linewidths; for these systems, the SC formulation gives a deeper transparency even in the linear regime, due to quantum-optical dephasing that is ignored by the SC model [11]. In our system, thermal dephasing dominates over this vacuum-field-induced dephasing. As the field is increased, however, the quantum-optical dephasing increases and eventually becomes comparable to the thermal linewidth, resulting in a small disagreement between our CQED and SC predictions at moderate fields.

We next consider the system response to a Gaussian pulse,  $E(t)$ , that has a 20 fs full width at half the maximum intensity and a center frequency,  $\hbar\omega = 2.042$  eV, resonant with the plasmon and exciton. Transient spectra obtained by Fourier transformation of the time-domain response are shown in Figure 3. At low intensities, the transient spectrum is identical to the linear steady-state spectrum. Strikingly, however, at certain higher fluences the resonant dip reverses to form a narrow spike. The corrected SC model remains in

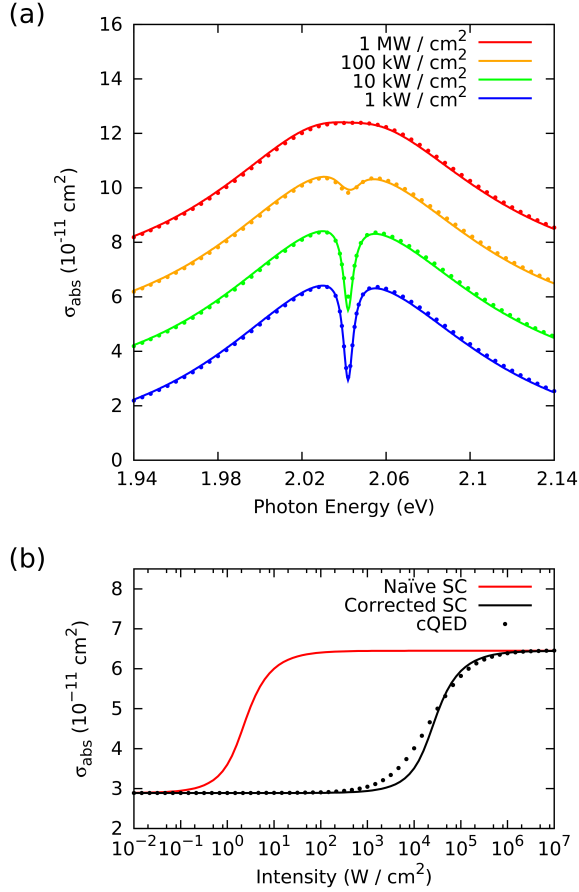


FIG. 2. (a) Steady-state absorption spectra calculated using the CQED (dots) and corrected SC (solid) model for various incident intensities. Successive spectra are displaced vertically by  $2 \times 10^{-11} \text{ cm}^2$ . (b) Intensity dependence of steady-state absorption cross-sections calculated using the CQED, naïve SC and corrected SC steady-state models, at a photon energy of 2.042 eV.

excellent agreement with the CQED model. As the pulse fluence increases beyond the range that is readily computable using the CQED model, the SC model predicts recurrences of the ultrafast reversal suggestive of Rabi oscillations.

The ultrafast reversals of the Fano resonance arise from the transient phase relationships of the plasmon and QD dipoles with respect to the incident light, as illustrated in Fig. 4. At the beginning of the incident pulse, as at steady state, the plasmon lags the driving laser by the  $\pi/2$  phase difference expected for a resonant oscillator [15]. The QD is driven primarily by the plasmon and thus lags the laser by an additional  $\pi/2$  phase difference. At low fluence, this phase relationship continues until the pulse is complete and the short-lived plasmon has

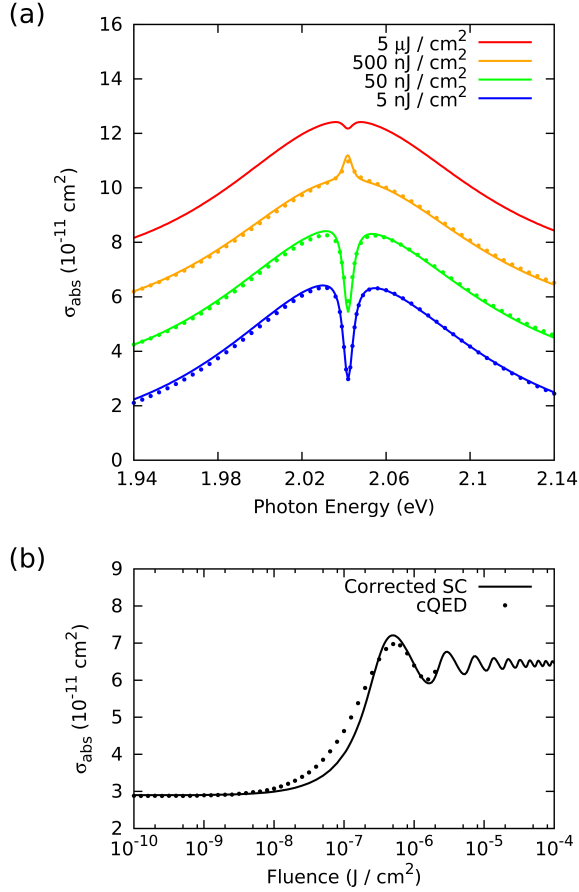


FIG. 3. (a) Absorption spectra calculated using the CQED (dots) and corrected SC (solid) models, for ultrafast pulsed excitation. Successive spectra, corresponding to varying fluences, are displaced vertically by  $2 \times 10^{-11} \text{ cm}^2$ . (b) Fluence dependence of the absorption cross-section for ultrafast pulsed excitation, calculated using the CQED and SC models, at a photon energy 2.042 eV.

decayed. Then, the longer-lived QD, still oscillating with a  $\pi$  phase lag relative to the laser, drives the plasmon; the plasmon thus acquires a  $\pi + (\pi/2) = (3\pi/2)$  phase lag, partially canceling its earlier oscillations in the spectral domain and producing the observed linear Fano dip. By contrast, at higher fluences, the QD population exhibits Rabi oscillations, reaching unity and then coherently being driven back down. This reverses the sign of the QD dipole [26], so that the lag of the QD phase relative to the laser is now zero. The phase frustration that previously led to transparency is replaced by a constructive interference that leads to induced absorption or superscattering.

Ultrafast reversal is thus due to a change in the phase of the coherent interaction between

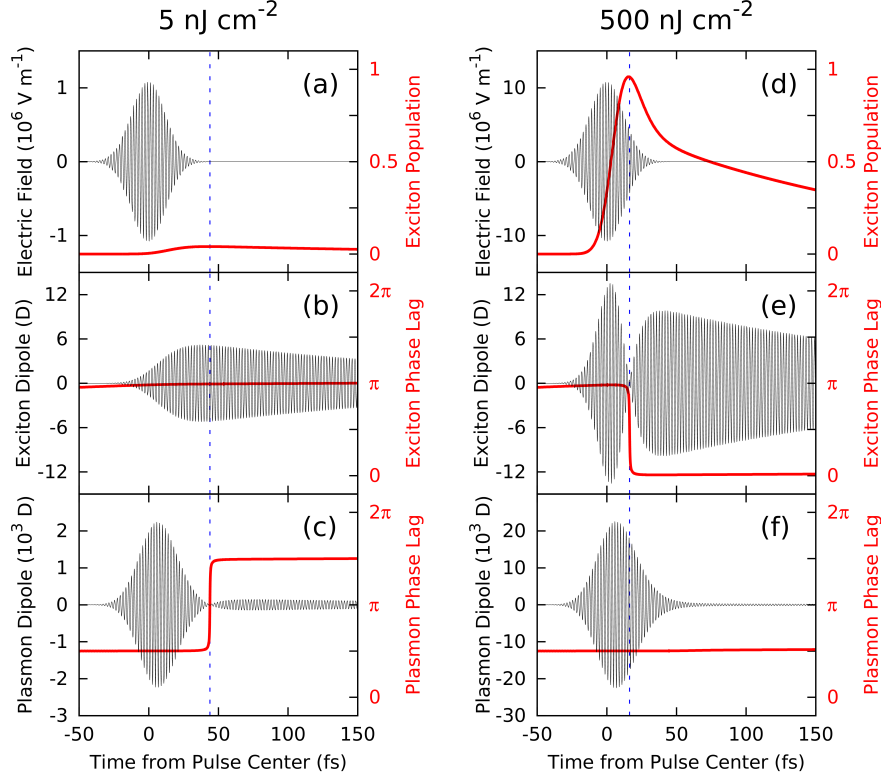


FIG. 4. Time evolution of the QD-plasmon system under pulsed excitation, calculated using the CQED model for two fluences. (a,d) Pulse's electric field and QD population. (b,e) QD's dipole and phase lag relative to the pulse. (c,f) Plasmon's dipole and phase lag. Dashed lines indicate times at which a phase jump occurs.

the QD and the plasmonic metal nanostructure. A similar change has been demonstrated in plasmonic or metamaterial systems that exhibit Fano resonances due to the coupling between bright modes and dark modes [27]. In this case, the sign of the interference can be controlled through careful selection of the linewidths and coupling strengths [28], or by adding a retardation-based phase delay [29]. Similarly, a change from steady-state transparency to enhanced absorption has been predicted in coupled QD-plasmon systems by changing the size of the metal nanoparticle and the detuning [15]. In these systems, reversal from destructive interference to constructive interference can be controlled only statically, by changing the structure of the system. In our QD-plasmon system, by contrast, the reversal can be controlled dynamically, by changing the fluence of the incident ultrafast pulses.

Not all QD-plasmon systems that exhibit Fano resonances will exhibit ultrafast reversal.



The reversal requires that the QD dipole oscillates significantly longer than the plasmon's intrinsic lifetime. In other words, we require  $\gamma_1^{\text{eff}} \ll \gamma_s$ , which implies  $g \ll \gamma_s/2$ . However,  $g$  must also be large enough to give a Fano resonance, which requires  $g \geq \sqrt{\gamma_s \gamma_2}/4$  [5, 18]. These constraints are more easily satisfied for  $\gamma_2 \ll \gamma_s$ . The large  $\gamma_s$  afforded by a lossy plasmonic component points to the intrinsically plasmonic nature of ultrafast reversal: such constraints are unlikely to be satisfied by a high-finesse photonic resonator.

Sufficiently narrow QD linewidths can be obtained by cooling to liquid-nitrogen temperatures, even if we account for absorption-induced heating of the plasmonic nanostructure. Achieving the required coupling strengths is a greater experimental challenge, but should be feasible using chemically synthesized components and directed assembly, such as DNA-based assembly of colloidal QDs and metal nanoparticles [30]. The availability of low-cost assembly methods is an advantage for these systems as compared to traditional CQED systems, which require complex and expensive top-down fabrication [31, 32].

Our treatment of the optical response of coupled QD-metal nanostructure systems has employed a larger thermal dephasing rate for the QD than has generally been considered in previous treatments. Although this means that certain phenomena requiring a high degree of coherence are suppressed, significant quantum-optical effects remain. First, the saturation of the Fano resonance is the principal optical nonlinearity at steady state, and the intensity at which this saturation occurs is due to a balance between two inextricable aspects of QD-plasmon coupling: plasmonic field enhancement lowers the incident fields required for saturation, while the Purcell effect increases the required fields. Second, we predict that the Fano resonance can undergo a reversal, changing from a transparency dip into a superscattering spike, when excited by femtosecond laser pulses with appropriate fluence. This ultrafast reversal represents a new means to coherently control optical interactions among nanostructures.

We thank Dr. Lina Cao for helpful conversations. This research was funded by the National Science Foundation (CHE-1059057). R. A. S. was supported by a National Science Foundation Graduate Research Fellowship. Use of the Center for Nanoscale Materials was supported by the U. S. Department of Energy, Office of Science, Office of Basic Energy Sciences User Facility, under Contract No. DE-AC02-06CH11357.

---

\* gray@anl.gov

- [1] M. Pelton, J. Aizpurua, and G. Bryant, *Laser Photon. Rev.* **2**, 136 (2008).
- [2] V. Giannini, A. I. Fernández-Dominguez, S. C. Heck, and S. A. Maier, *Chem. Rev.* **111**, 3888 (2011).
- [3] T. Ming, H. Chen, R. Jiang, Q. Li, and J. Wang, *J. Phys. Chem. Lett.* **3**, 191 (2012).
- [4] W. Zhang, A. O. Govorov, and G. W. Bryant, *Phys. Rev. Lett.* **97**, 146804 (2006).
- [5] X. H. Wu, S. K. Gray, and M. Pelton, *Opt. Express* **18**, 23633 (2010).
- [6] E. Waks and J. Vuckovic, *Phys. Rev. Lett.* **96**, 153601 (2006).
- [7] R. D. Artuso and G. W. Bryant, *Nano Lett.* **8**, 2106 (2008).
- [8] R. D. Artuso and G. W. Bryant, *Phys. Rev. B* **82**, 195419 (2010).
- [9] R. D. Artuso, G. W. Bryant, A. Garcia-Etxarri, and J. Aizpurua, *Phys. Rev. B* **83**, 235406 (2011).
- [10] M.-T. Cheng, S.-D. Liu, H.-J. Zhou, Z.-H. Hao, and Q.-Q. Wang, *Opt. Lett.* **32**, 2127 (2007).
- [11] E. Waks and D. Sridharan, *Phys. Rev. A* **82**, 043845 (2010).
- [12] W. Zhang and A. O. Govorov, *Phys. Rev. B* **84**, 081405 (2011).
- [13] A. Ridolfo, O. Di Stefano, N. Fina, R. Saija, and S. Savasta, *Phys. Rev. Lett.* **105**, 263601 (2010).
- [14] A. Manjavacas, F. J. G. de Abajo, and P. Nordlander, *Nano Lett.* **11**, 2318 (2011).
- [15] X.-W. Chen, V. Sandoghdar, and M. Agio, *Phys. Rev. Lett.* **110**, 153605 (2013).
- [16] A. Trügler and U. Hohenester, *Phys. Rev. B* **77**, 115403 (2008).
- [17] L. Verslegers, Z. Yu, Z. Ruan, P. B. Catrysse, and S. Fan, *Phys. Rev. Lett.* **108**, 083902 (2012).
- [18] See Supporting Information.
- [19] R. W. Ziolkowski, J. M. Arnold, and D. M. Gogny, *Phys. Rev. A* **52**, 3082 (1995).
- [20] J. A. Gruetzmacher, R. A. Nome, A. M. Moran, and N. F. Scherer, *J. Chem. Phys.* **129**, 224502 (2000).
- [21] C. Wang and R. Vyas, *Phys. Rev. A* **55**, 823 (1997).
- [22] L. Novotny and B. Hecht, *Principles of Nano-Optics* (Cambridge, 2006).
- [23] B. T. Draine and P. J. Flatau, *J. Opt. Soc. Am. A* **11**, 1491 (1994).

- [24] L. Besombes, K. Kheng, L. Marsal, and H. Mariette, *Phys. Rev. B* **63**, 155307 (2001).
- [25] G. Nienhuis and C. T. J. Alkemade, *Physica C* **81**, 181 (1976).
- [26] R. W. Boyd, *Nonlinear Optics*, 3rd ed. (Elsevier, 2008).
- [27] B. Luk'yanchuk, N. I. Zheludev, S. A. Maier, N. J. Halas, P. Nordlander, H. Giessen, and C. T. Chong, *Nat. Mater.* **9**, 707 (2010).
- [28] P. Tassin, L. Zhang, R. Zhao, A. Jain, T. Koschny, and C. M. Soukoulis, *Phys. Rev. Lett.* **109**, 187401 (2012).
- [29] R. Taubert, M. Hentschel, J. Kästel, and H. Giessen, *Nano Lett.* **12**, 1367 (2012).
- [30] E. Cohen-Hoshen, G. W. Bryant, I. Pinkas, J. Sperling, and I. Bar-Joseph, *Nano Lett.* **12**, 4260 (2012).
- [31] D. Englund, A. Faraon, I. Fushman, N. Stoltz, P. Petroff, and J. Vuckovic, *Nature* **450**, 857 (2007).
- [32] I. Fushman, D. Englund, A. Faraon, N. Stoltz, P. Petroff, and J. Vuckovic, *Science* **320**, 769 (2008).